AD_____

Award Number: W81XWH-05-1-0363

TITLE: Miniature and Molecularly Specific Optical Screening Technologies for Breast Cancer

PRINCIPAL INVESTIGATOR: Nirmala Ramanujam

CONTRACTING ORGANIZATION: Duke University
Durham, NC 27705

REPORT DATE: October 2011

TYPE OF REPORT: Final

PREPARED FOR: U.S. Army Medical Research and Materiel Command
Fort Detrick, Maryland 21702-5012

REPORT DOCUMENTATION PAGE

Form Approved
OMB No. 0704-0188

1. REPORT DATE *(DD-MM-YYYY)*	**2. REPORT TYPE**	**3. DATES COVERED** *(From - To)*
01-10-2011	Final	1 SEP 2005 - 31 AUG 2011

4. TITLE AND SUBTITLE
Miniature and Molecularly Specific Optical Screening Technologies for Breast Cancer

5a. CONTRACT NUMBER

5b. GRANT NUMBER
W81XWH-05-1-0363

5c. PROGRAM ELEMENT NUMBER

6. AUTHOR(S)
Nirmala Ramanujam

E-Mail: nimmi@duke.edu

5d. PROJECT NUMBER

5e. TASK NUMBER

5f. WORK UNIT NUMBER

7. PERFORMING ORGANIZATION NAME(S) AND ADDRESS(ES)
Duke University
Durham, NC 27705

8. PERFORMING ORGANIZATION REPORT NUMBER

9. SPONSORING / MONITORING AGENCY NAME(S) AND ADDRESS(ES)
U.S. Army Medical Research and Materiel Command
Fort Detrick, Maryland 21702-5012

10. SPONSOR/MONITOR'S ACRONYM(S)

11. SPONSOR/MONITOR'S REPORT NUMBER(S)

12. DISTRIBUTION / AVAILABILITY STATEMENT
Approved for Public Release; Distribution Unlimited

13. SUPPLEMENTARY NOTES

14. ABSTRACT

The goal of this proposal is to harness the power of light to create "miniature and molecularly specific optical technologies" for breast cancer diagnosis and detection. The miniature technologies will leverage on millimeter scale silicon detectors and LEDs to make compact devices that can be used in a practical clinical setting for breast cancer detection. The features that will be exploited for optical detection/diagnosis of breast cancer will include the physiological, structural and molecular alterations that accompany the transformation of a cell from a normal to malignant state. This proposal also focuses on using contrast agents, specifically aminolevulinic acid (ALA) induced protoporphyrin IX (PpIX) and NBDG, for the molecular detection of breast cancer.

15. SUBJECT TERMS
optical, spectroscopy, imaging, fiber-optic, molecular, screening

16. SECURITY CLASSIFICATION OF:			**17. LIMITATION OF ABSTRACT**	**18. NUMBER OF PAGES**	**19a. NAME OF RESPONSIBLE PERSON**
a. REPORT	**b. ABSTRACT**	**c. THIS PAGE**			USAMRMC
U	U	U	UU	28	**19b. TELEPHONE NUMBER** *(include area code)*

Table of Contents

1. INTRODUCTION

The objective of this proposal is to harness the power of light to create “miniature and molecularly specific optical technologies” for the eradication of breast cancer. Specifically this application focuses on a system on a chip device to detect molecularly specific sources of optical contrast for breast cancer. Both intrinsic (hemoglobin saturation, total hemoglobin content, reduction-oxidation ratio) and extrinsic sources of optical contrast (specifically aminolevulinic acid (ALA) induced protoporphyrin IX (PpIX) and 2-[*N*-(7-nitrobenz-2-oxa-1,3-diazol-4-yl)amino]-2-deoxy-D-glucose (2-NBDG) will be studied for breast cancer imaging. These sources of contrast coupled with the system on a chip device will be initially used for intraoperative margin assessment and predicting/evaluating response to therapy. Once we have established the feasibility of using this technology in the margin assessment and therapy application, we will focus on applications that focus on early detection, including core needle biopsy and ductoscopy, which require further modifications to the technology.

2.1 Body Project 1: System-on-a-chip device

A. Original SOW for five years

1) *To establish the design specifications of the first-generation system-on-a-chip device.* This aim will involve throughput calculations and Monte Carlo modeling to determine the signal-to-noise ratio that can be achieved with the nano scale sources and detectors, and the experimental evaluation of the signal-to-noise of the test system on turbid “tissue-like” media. The signal-to-noise ratios achieved with the test system will be quantitatively compared to that achieved with a standard bench top system (year 1).
2) *To engineer and test the first-generation system-on-a-chip device.* The knowledge base derived from aim 1 will be used to engineer a first generation system-on-a-chip device and the performance of the device will be characterized on synthetic tissue phantom models. The signal-to-noise ratio and fluorescence attenuation characteristics of the system-on-a-chip device will be compared to that of a standard bench top counterpart (year 2).
3) *To experimentally establish the signal-to-noise ratio with which the system-on-a-chip device can measure the fluorescence of ex vivo human breast tissues.* The system-on-a-chip device will be used to measure the fluorescence properties of 25 pair of malignant and non-malignant breast tissues excised from approximately 25 patients undergoing breast cancer surgery. The results obtained from this study will be quantitatively compared to benchmarks established by our bench top counterpart, which has been shown to measure breast tissue fluorescence with excellent signal-to-noise ratio (year 3).
4) *To test the feasibility of implementing optical spectroscopy via a ductoscope.* The system-on-a-chip device will be incorporated into a standard ductoscope. The ductoscope will be used to measure the fluorescence properties of 25 pair of malignant and non-malignant breast tissues excised from approximately 25 patients undergoing breast cancer surgery (years 4-5).

B. Summary of accomplishments in year 1

In year 1, we have completed the main goals of the SOW for year 1. The major achievements include thermal modeling of the heat dissipation effects of compact LEDs on tissue samples, selection of multi-wavelength compact light sources, calculating bandwidth effects of broadband light sources (such as LEDs) on the RMS errors for the extracted tissue optical and physiological properties, selection of photodiodes, and the design and testing of various single-

pixel probe prototypes (P1 and P2 as shown in Figure 2.1). The major deviation from the SOW is that we used commercially available light sources and detector in our design, instead of using nano scale sources.

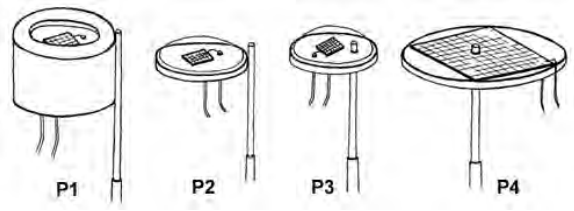

Figure 2.1. Conceptual drawings of four single-pixel probe geometries P1-P4.

C. Summary of accomplishments in year 2

In year 2, we used knowledge base derived from year 1 to build more first generation single-pixel devices using an optical fiber for illumination and photodiodes for the collection of diffusely reflected light from a tissue sample. In particular, we have built single-pixel probes of different illumination and detection geometries named as P3-1 (600 μm fiber), P3-2 (1 mm fiber), P4-1 (600 μm fiber), and P4-2 (1 mm fiber), as shown in Figure 2.1, all using and 2.4 mm photodiode. P3-1 and P3-2 were tested in synthetic tissue phantoms with known optical properties, and their experimental diffuse reflectance spectra were compared with those of a forward Monte Carlo model.

We have also extracted the phantom optical properties from the diffuse reflectance spectra obtained from a tunable light source using an inverse Monte Carlo (MC) model. For P3-2, we found that the overall errors for quantifying the absorption and scattering coefficients were 6.0±5.6% and 6.1±4.7%, respectively. These results are comparable with those achieved with our bench-top system which has an overall error 5.8±5.1% and 3.0±3.1% for extracting μ_a and μ_s', respectively. A short paper on P3-2 has been accepted for publication by the Journal of Biomedical Optics Letters [1] and a copy of the manuscript is attached to this report. Phantom optical properties with reduced number of wavelengths were also extracted and compared to that of the bench-top system with all wavelengths.

In year 2, a clinical study conducted by our group using the bench-top system and the MC model showed that DRS alone has achieved comparable sensitivity and specificity for discriminating malignant from nonmalignant breast tissues as combined reflectance and fluorescence spectroscopy[2]. Therefore, our research in this miniature device has been focused mainly on diffuse reflectance spectroscopy (DRS) for breast cancer diagnosis and tumor margin assessment.

D. Summary of accomplishments in year 3

In year 3, we have modified the probe geometries of the single-pixel probe developed in year 2 in order to increase the signal-to-noise ratio of the probe and to be able to extract a much larger range of optical properties than those of the probes built in year 2. The new probe was tested in synthetic tissue phantoms over a wide range of absorption and reduced scattering coefficients, and the phantom optical properties were extracted from the diffuse reflectance spectra obtained from the tunable light source and new probe with the inverse MC model previously developed by our group. Using the same phantom data collected by our new probe, optical properties with a reduced number of wavelengths were extracted to assess the feasibility of replacing the

tunable light source with several smaller LEDs to further reduce the size and cost of the current system. In addition, cross-talk analysis was performed as a first step to multiplex the single pixel system into an imaging system that can quantify tissue physiological and morphological properties over a large tissue area. We have also fabricated a 3x3 fiber-photodiode array for test in the lab.

Although the original goals of the SOW is to use the system-on-a-chip device to measure the fluorescence properties of 25 pair of malignant and non-malignant breast tissues excised from approximately 25 patients undergoing breast cancer surgery, we understand that many challenges exist and it may take a relatively long time to reach this goal. As an intermediate step, the work in year 3 has been focused on partially miniaturizing the current bench-top system. This miniaturized probe preserves the potential for multiplexing that can be used for spectral imaging of tissue while uses all the wavelengths available to the bench-top system.

In year 3, a poster on the single-pixel device titled "A Miniature Optical Device for Noninvasive, Fast Characterization of Tumor Pathology," was presented to the 2008 OSA Topic Meeting in Biomedical Optics**,** March 16-19, 2008, St. Petersburg, Florida. A journal paper titled "Cost-effective diffuse reflectance spectroscopy device for quantifying tissue absorption and scattering in vivo," was also published in Journal of Biomedical Optics Letters in 2008.

E. Summary of accomplishments in year 4

In year 4, the single-pixel probe (using a 5.8x5.8 mm Si detector) with fiber-based illumination developed in year 3 have been expanded to a 3x3 spectral imaging (FISI) array. A FISI system was constructed using the 3x3 array and an 8-wavelength xenon light source. The FISI system was tested in a number of homogeneous liquid phantoms with optical properties representative of breast tissue and excellent accuracy was achieved in extraction of the phantom optical properties. This demonstrated the possibility of performing spectral imaging with low cost photodiodes and 8 LEDs covering the wavelength range from 400 – 600 nm. To further reduce the size and cost and to simplify the probe fabrication, we have proposed a new back-illumination strategy to replace the fiber-based illumination. A single-pixel version of the back-illuminated probe (using a 2.4x2.4 mm Si detector) was built and tested and the performance was found to be comparable to those of the FISI array and the current clinical system. A 4x4 back-illuminated spectral imaging (BISI) array has also been designed and the optimization and testing will be performed in year 5. The drilled commercial Si detectors are good for proof-of-concept study, but our long term goal is to build a system-on-a-chip spectral imaging device, which requires the integration of photodiodes, light delivery network and electronics on to a single wafer. In year 4, we have also made initial GaAs photodiode arrays that will be improved and optimized in year 5.

In year 4, a peer reviewed journal article titled "A strategy for quantitative spectral imaging of tissue absorption and scattering using light emitting diodes and photodiodes" was published in *Optics Express* (Opt Exp 17 (3):1372-1384, 2009). A poster on the 3x3 FISI system titled "A Reduced-Cost Spectral Imaging System for Breast Tumor Margin Assessment," was presented to ECI conference on Advances in Optics for Biotechnology, Medicine, and Surgery XI. Burlington, VT, USA, June 2009.

F. Summary of accomplishments in year 5

In year 5, we have modified the Monte Carlo inverse model for reflectance to account for reduced number of wavelength and bandwidth effects. This improved MC model will enable us

to replace the expensive Xe light source with a filter wheel with a handful of low-cost LEDs, making is possible to build a very compact quantitative spectral imaging device that can be used for intra-operative tumor margin assessment. Our phantom experiments with the 4x4 BISI array indicated that it is feasible to perform quantitative imaging of heterogeneous samples with the device, but the throughput, illumination uniformity, and fabrication processes need to further improvement for better accuracy and repeatability. We hope the new design of the 4x4 array will help us to achieve these goals in the no cost extension year (year 6). In the meantime, we have also modified the Monte Carlo model of reflectance for heterogeneous media, which will allow us to simulate imaging arrays with significant crosstalk among adjacent pixels and thus improving the spatial resolution of the device.

G. Progress report for year 6

In year 6, we explored the lithographically defined aperture arrays as described from the year 5 progress report, shown in Figure 2.2. The rationale was that with larger slits that act as apertures adjacent to circular detectors, the system would have higher throughput and SNR. However, we found very early on that because the slits sat on a lower plane than the detectors themselves, much of the photons were likely scattered by the metals or absorbed by the dark, opaque edges of the photodetector dyes. In short, we were unable to achieve the SNR necessary for further investigation for this strategy.

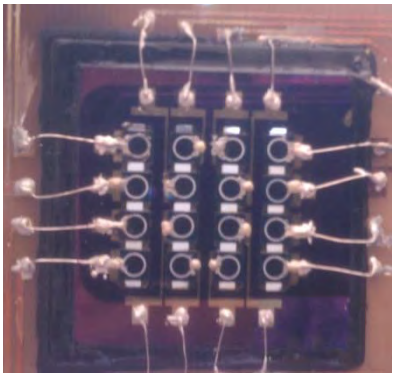

Figure 2.2 – 4x4 BISI array with lithographically defined apertures

Revised SOW:

Because we were unable to achieve the throughput and SNR with the design proposed for year 6, we made the following revisions to complete the work of this grant:

- To fabricate and test new custom annular photodiode arrays, which allows for a significant improvement in geometrical uniformity
- To design and test a new light delivery strategy via a planar waveguide, which allows for better illumination uniformity compared to the previous free-space illumination
- To incorporate and test a new current amplifier, which improves SNR of the system
- To develop a systematic method for optimizing and selecting wavelengths for this application
- To test the detector arrays in biological tissue for SNR and show feasibility for clinical use

In year 6, we have made significant progress in each of the following areas:

(a) In-house fabrication of custom annular photodiode arrays

For the previous 5 years, we purchased commercially available photodiodes to test the concept of using such inexpensive detectors for the purposes of spectroscopic imaging of tissue. We found that the best geometry for maximizing throughput and SNR is an annular detector in which light exits the central aperture. Because our Monte Carlo model accurately tracks the paths of photons in turbid media based on probe geometry, optical properties of tissues, among other parameters, we ran into problems with modeling the detectors accurately after we manually drilled an aperture in the centers of each detector. We were able to show proof-of-concept on single-pixel versions of such detectors in two publications (Yu B, *JBO* 13, 2008 and Lo JY, *Optics Express* 2009), however when multiplexed into a 4x4, the modeling became tedious and unpractical. We also attempted to circumvent the need for fabricating detectors in-house by proposing the slit geometry array at the end of year 5. While it helped with uniformity, we suffered from SNR. In year 6, we have successfully fabricated custom annular photodiode arrays in-house and tested the photodiodes for photosensitivity and compared this to the previous commercially available detectors from Hamamatsu.

The photodiodes (PD) were fabricated on an n-type epitaxial Si sample consisting of: 7 μm *n*-Si (epitaxial, P doped, 5-9 Ω-cm)/ 600 μm *n*-Si (substrate, Sb doped, 0.025-0.045 Ω-cm). A boron doped spin-on glass (SOG) (Emulsitone, Borosilicafilm 5 x 10^{19} cm^{-3}) was diffused into the epitaxial layer to create the p-type material to define the *pn* junction. A phosphorous doped SOG film (Emulsitone, Phosphoro-silicafilm 5 x 10^{20} cm^{-3}) was coated on the back of the Sb-doped substrate and annealed to form the n+ back contact layer. Standard lithography was used to define the top dual-ring Al ohmic contact and a blanket Al/Pt layer was deposited to form the back contact. Deep reactive ion etching (SPTS Pegasus) was performed to etch the 0.75 mm wide and 600 μm deep apertures in the PDs using the Bosch process. A 52 nm thick SiN layer deposited using plasma enhanced chemical vapor deposition (PECVD) formed an anti-reflection top coating on the array. The custom PD array was wire-bonded to a patterned FR4 board that had a circular cut out to match the PD array in the center, to enable illumination from the backside of the device. The wire bonds were potted in epoxy, since the samples were in contact with the surface of the imaging array. Figure 2.3 shows the images of the custom annular arrays that have well-defined geometries and importantly, the central aperture that we have found to be best for maximizing throughput and SNR.

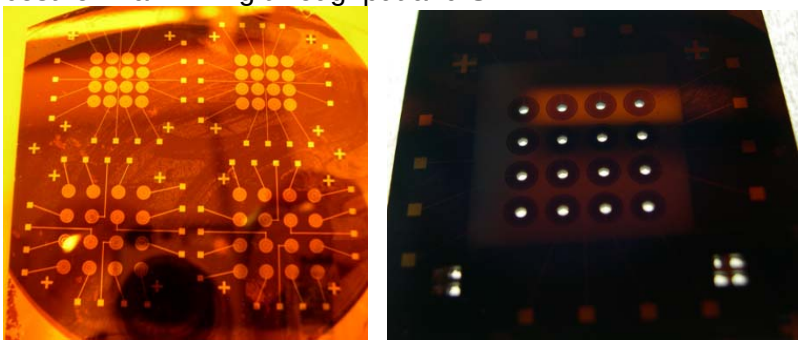

A B

Figure 2.3 – (A) photograph of 4 sets of 4x4 arrays with differing geometries. (B) photograph of a 4x4 array with after AR coating and apertures made with deep reactive ion etching

The custom imaging array consists of sixteen annular silicon *pn* junction PDs. The outer and inner diameters of these fabricated PDs were 2.5 mm and 0.75 mm, respectively. The center-to-center spacing of the PDs was 4.5 mm, enabling higher resolution imaging than the previously reported imaging system composed of commercial PDs, which was limited to a spacing of 7.5 mm – 8 mm. Figure 2.4 shows a more elegant 4x4 back-illuminated spectral imaging (BISI) probe that does not have mechanically drilled holes. The new array has significant advantages over all other arrays built in previous years in reproducibility, geometrical uniformity, and ease of modeling.

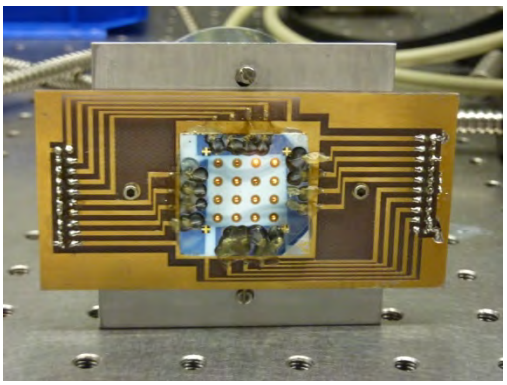

Figure 2.4 – photograph of 4x4 BISI incorporated with new custom annular photodiode array.

The fabricated imaging array was characterized using an eight channel source-measuring unit (Keithley SMU-4200) with a switch box that enabled testing all 16 detectors. The PDs were characterized with normal illumination to measure the photoresponse with a Xenon arc lamp with the following filters applied: 400, 420, 440, 470, 500, 530, 570, 600 nm. The typical responsivity of the detectors were measured to be 0.18 – 0.38 A/W for 400-600 nm. The dark currents of the detectors were 65 – 200 pA. Like its predecessors, this new 4x4 array has "leakage" signals in the absence of true diffuse reflectance signal because of the photocurrents generated due to the backside source illumination incident on the inner edge of the apertures. The previously drilled 4x4 arrays have leakage currents as high as 5-50 nA. This new custom array has leakage currents of less than 2.5 nA, likely because the apertures were not manually drilled (less unintended scattering), and are thinner (610 microns) with less surface area for possible photon collection along the edges. Figure 2.5 shows the performance of our custom PD array compared to that of an undrilled Hamamatsu photodetector. It is important to note that a drilled photodetector has worse performance than an undrilled detector. The comparison to the drilled detector was not made because of the inherent problem of not knowing the exact area of the active region. This problem is completely solved with the in-house fabrication of annular photodiode arrays.

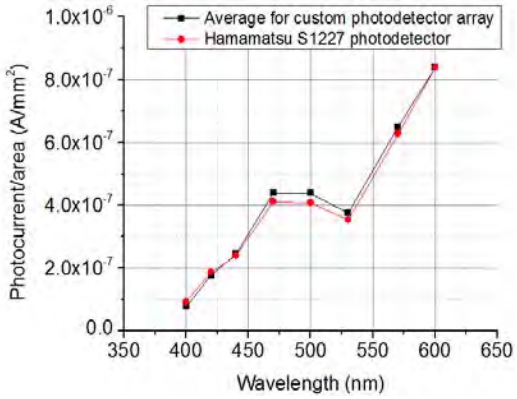

Figure 2.5 – Comparison of performance of custom PD array with an undrilled Hamamatsu photodetector

(b) Design and test of a planar waveguide for light delivery

In previous years of iterating on our system design, we have used fiber-based illumination strategy for the single pixel, non-imaging system, and have used a free-space back-illumination approach for the 4x4 array when optical fibers would have become too unwieldy for clinical use. However, the design struggled with throughput, SNR, and illumination uniformity. In year 6, we have developed an alternative strategy for light delivery.

The new light distribution sub-system for the quantitative diffuse reflectance spectroscopic array consists of a planar waveguide cavity with conical light deflectors arrayed on one surface of the waveguide cavity. These inverted cones serve to deflect a portion of the light trapped in the cavity to and through a set of 16 apertures (1 mm diameter) which reside on the opposing face as shown in Figure 2.6. Immediately below these apertures is positioned a photodetector array consisting of annular Si p-n junctions, with their apertures aligned with those of the waveguide cavity apertures. Light is deflected by the cones into and through the cavity and the photodetector apertures. This light is back scattered by the tissue specimen in contact with the structure – a portion of which is detected by the array of pn junctions which serve as the detector array.

The waveguide cavity is excited with a set of 6-9 solid state sources (LEDs, laser diodes, and diode-pumped solid state lasers– one for each of the 6-9 sampling wavelengths) brought together by a set of dichroic mirrors into a common output, which in turn illuminates a set of 4 optical fibers. These fibers are used to inject the light into the planar waveguide cavity. The waveguide cavity and cone structure are metalized in order to more efficiently trap and distribute the light through the circular apertures. The light sources are used to sample the diffuse reflectance spectrum of the tissue under study.

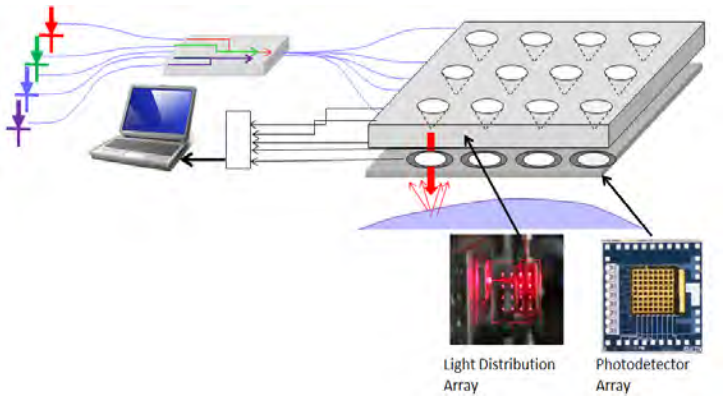

Figure 2.6 – Schematic overview of light distribution system

B1. Planar waveguide / photodiode array design

We have designed and analyzed several planar waveguide structure cavities as a function of light distribution efficiency and uniformity. Optical analysis is performed using using ZEMAX ray tracing software. Silver (Ag) was chosen as the reflective coating for the planar waveguide cavity because of its high reflectivity encompassing our wavelengths of interest (above 93% reflectivity from 450 nm to 800 nm). See Figure 2.7. The minimum Ag layer thickness to achieve essentially maximum reflectivity is ~ 120 nm.

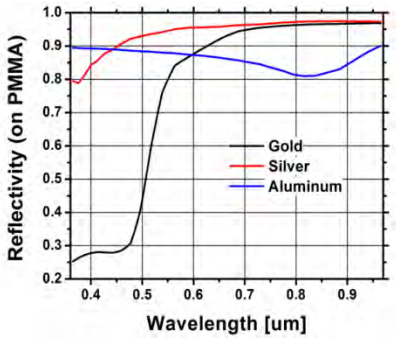

Figure 2.7 – Reflectivity vs. wavelength for the 3 candidate metals

Ray tracing modeling (via Zemax) was used to design the dimpled planar waveguide cavity for maximum optical throughput and aperture-to-aperture uniformity. Two photodetector array designs were studied: a stand-alone set of pn junctions fabricated in Si wafers of standard thickness (610 μm), and a second design in which the Si was thinned to 10 μm and then bonded to a glass support. As seen in Figure 2.8, regardless of the photodetector module material(s), the fraction of light exiting the 16 apertures decreases exponentially with an overall thicker module. Second, for a given total photodetector module thickness, higher throughput is obtained by sacrificing the photodetector glass support.

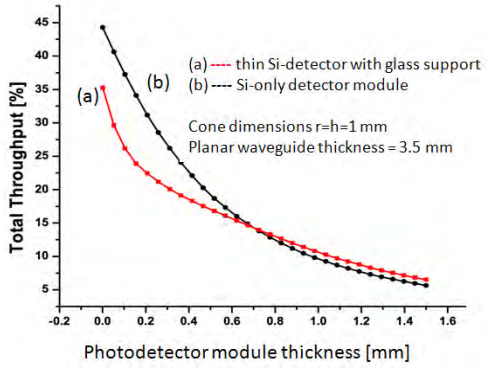

Figure 2.8 – Total throughput vs. photodetector module thickness

B2. Probe divergence and uniformity

All of the above geometries show approximately the same degree of aperture-to-aperture throughput variance and divergence uniformity. Figure 2.9 shows the calculated light intensity distributions vs. distance from the exit aperture for a typical waveguide cavity/photodetector structure: (a) at the Si detector aperture, (b) 1 mm below the exit aperture plane, and (c) 3 mm below the exit aperture plane. In this design, 95% of the array apertures will deviate less than ±10% (2σ/avg) from the average, and uniformity is achieved.

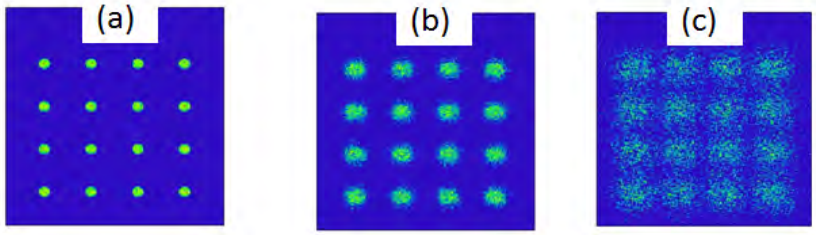

Figure 2.9 – Light intensity distribution for a 750 mm planar waveguide cavity with an all-Si photodetector module 500 microns thick. Detector planes at (a) 50 microns, (b) 1000 microns, and (c) 3000 microns.

A convenient approximation for the divergence of light from the apertures as a function of vertical distance from the aperture is given by:

$2\,R(z) \sim 2\,r_o + 2\,z\,\tan\theta_o$

where 2R(z) is the full width diameter of the intensity profile at $1/e^2$, $2r_o$ is the aperture diameter, and θ is the divergence half angle of the light . For the particular case of a 3.5 mm thick planar waveguide with cones r = h = 1 mm and an all silicon, 610 μm thick photodetector module, we find the full width divergence angle to be $\theta_o = 37°$.

B2. Planar waveguide / photodetector array alignment

Figure 2.10 depicts the method we will use to align both the input fibers and the photodetector array to the planar waveguide cavity. The carrier structure will allow us to mechanically support the input fibers and provide alignment feature for waveguide and photodetector plate. The ferrules allow us to terminate, polish, and protect the fiber ends.

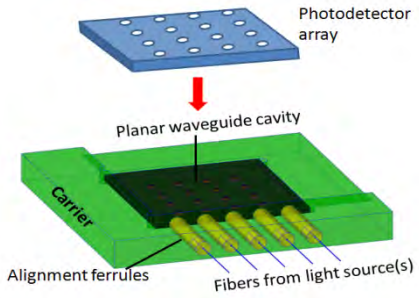

Figure 2.10 – Self-aligning waveguide support

B3. Alternative light sources

Table 1 is a summary of our survey of optical sources suitable for the system. Vendors should be able to supply any visible wavelength we require.

Table 1: Survey of LEDs, laser diodes, and DPSS lasers

Type	**LED**	**Laser Diode**	**DPSS**
Wavelengths	UV – VIS – IR	VIS – IR	UV – VIS – IR
Bandwidth ($\Delta\lambda_{1/2}$)	> 15 nm	< 6 nm	< 3 nm
Optical power	~ 0.5 - 1 W	~ 50 mW	~ 100 mW
Package Size	10 – 30 mm	5.6, 9 mm metal can	< 30 x 30 x 150 mm
Fiber Coupling	Pigtail available	Pigtail available	Pigtail available
Beam FWHM	> 150°	< 10° x 35°	< 1.5 mrad
Approx. Cost	< $10	$20 - $3000	$150 - $12,000
Pros	• inexpensive • Wide bandwidth	• Very compact packages available • Narrow bandwidth	• no external current source needed • integral heat sink • very narrow bandwidth
Cons	• Relatively inefficient fiber coupling • Requires external current supply • Heat sink needed for high powers	• Scarce 532-635 nm • Requires external current supply • Asymmetric beam divergence • Heat sink needed for high powers	• Bulky package • More expensive

(c) Improving SNR with new current amplifier design

In addition to improving throughput and SNR with our new light delivery strategy, we worked to improve the current amplifier to be incorporated into the final system. In our previous single pixel versions of the system, we had used a low-noise current amplifier (PDA-750, Terahertz Technologies Inc.) for measuring photocurrent generated by the photodiode. When we expanded to a 4x4 probe for imaging, we used a multi-channel transimpedance amplifier (Multiboard, SolGel Technologies GmbH) so that the signals can be read simultaneously. The transimpedance amplifier circuitry was assembled within a small metal housing and powered using a commercial 12V power supply. The output voltage was read and transmitted to a laptop using a USB-controlled data acquisition card (NI USB-6210, National Instruments). We found

that this multi-channel amplifier had a noise level on the order of tens of nA. The photocurrent generated from the single-pixel probes ranged from nA to µA of power. Thus, we were unable to measure or perform testing on liquid phantoms with average μ_a (400-600 nm) greater than 2/cm.

We started designing a new integrateded transimpedance amplifier (ITIA) array, which will also have multplexed ADC modules. The ITIAs will be surface mount soldered to a compact printed circuit board located close to the detector array to minimize noise in the sensitive detector current signal lines. A schematic of a 16-channel ITIA that will be used to read the photocurrent of a 4x4 array is shown in Figure 2.11, and the specifics of the circuitry of the ITIA is shown in Figure 2.12. Initial testing has been done on a single-channel ITIA circuit. The ITIA produces an appropriate output for currents ranging from 1 nA to 6 µA. Figure 2.13 also shows the linearity range of the ITIA, which is between 2 nA and 12 µA.

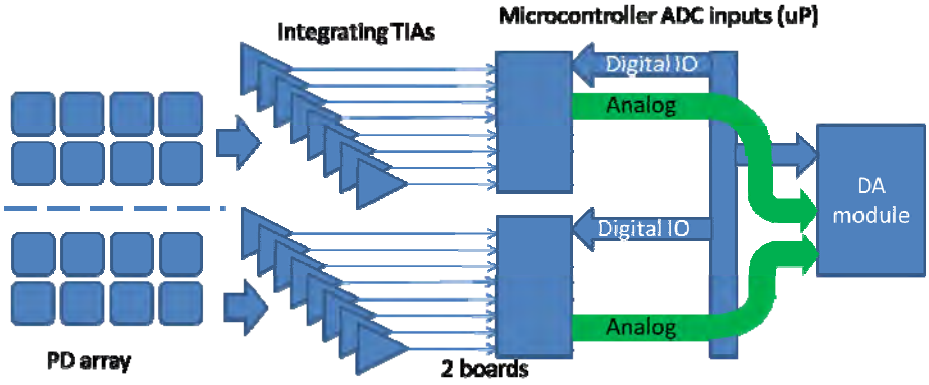

Figure 2.11 – Schematic of 16-channel ITIA design

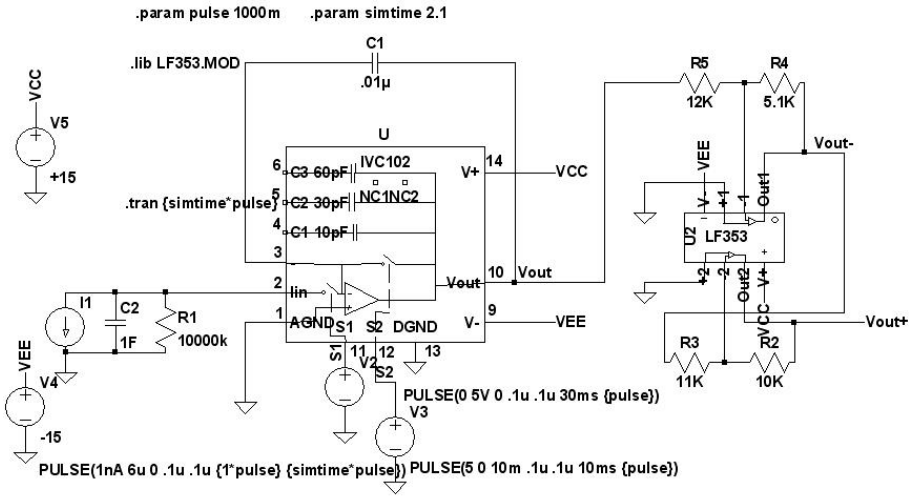

Figure 2.12 – Circuitry of ITIA design

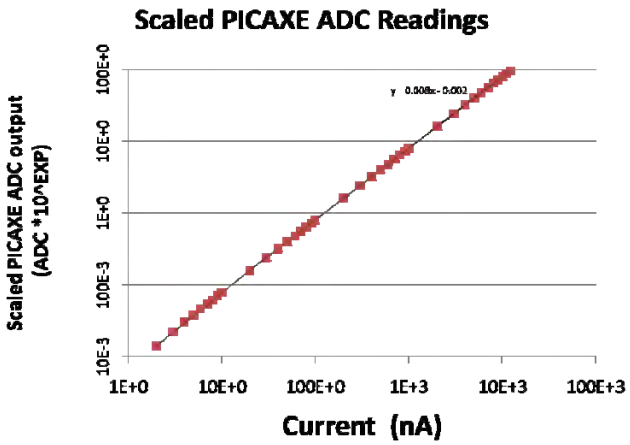

Figure 2.13 – Linearity testing of single-channel ITIA

We connected a single-channel ITIA to one corner pixel (lowest throughput ~4-6 μW) of the fabricated 4x4 annular detector array, and we tested the pixel for SNR in liquid phantoms comprised of India ink and intralipid. In a phantom that simulates the optical properties of malignant tissue (μ_a = 20.34/cm and μ_s' = 9.5/cm at 450 nm), we achieved an SNR between 40-60 dB from 440-600 nm. The next step is to expand the ITIAs into 16 circuits.

(d) Wavelength selection conducted with a genetic algorithm

We previously used an empirical method for selecting the wavelengths of filters and/or LEDs to be used in the system based phantom studies consisting of powdered hemoglobin and crocin (to simulate beta carotene, an absorber present in adipose tissue). In year 6, we developed a systematic method for selecting these discrete center wavelengths based on (1) the biological molecules to be measured (total hemoglobin content, beta carotene, etc), (2) the wavelengths and sources that are commercially available, and (3) optical contrast that will provide diagnostic information, i.e. hemoglobin, tissue oxygenation, etc.

A genetic algorithm available from MATLAB optimization toolbox was used to perform the wavelength selection. A Monte Carlo simulation of diffuse reflectance was performed to generated reflectance spectra of various tissue types, ranging from adipose tissue to malignant tissue, all with varying optical properties. The inverse Monte Carlo algorithm was used to extract optical properties from those reflectance spectra. The genetic algorithm works by minimizing the errors of these extractions. Figure 2.14 shows an example of how the optimization works by minimizing the fitness criteria (extraction errors) over the many iterations of wavelength selection. The initial, randomized wavelength sets have high overall errors. The genetic algorithm continues by keeping the best sets of wavelengths and generating additional sets of wavelengths from those previous sets of wavelengths with the lower extraction errors. The process is iterative, and the last generation of wavelengths should contain the best solution.

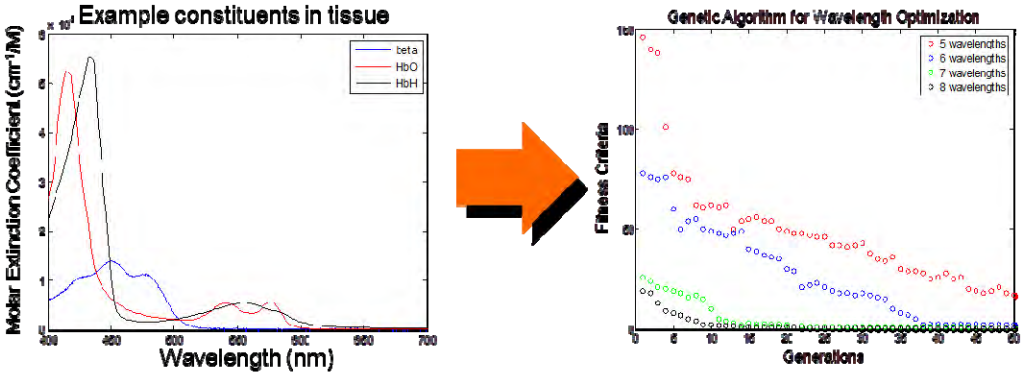

Figure 2.14 – Example of optimization performed to select a set of wavelengths to extract 3 absorbers with high accuracy.

Figure 2.15 shows the feasibility of extracting tissue data with a reduced wavelength number. With 8 bandpass filters at 440, 450, 460, 490, 550, 580, 590, 600 nm and a 10 nm FWHM, we are able to achieve correlation coefficients of the normal and tumor samples at 0.95 and 0.89, respectively. The bandpass filters that we had arrived at empirically, 400, 420, 440, 470, 500, 530, 570, 600 nm that we have used in previous generations of this system is unable to perform as well (< 0.7 for both).

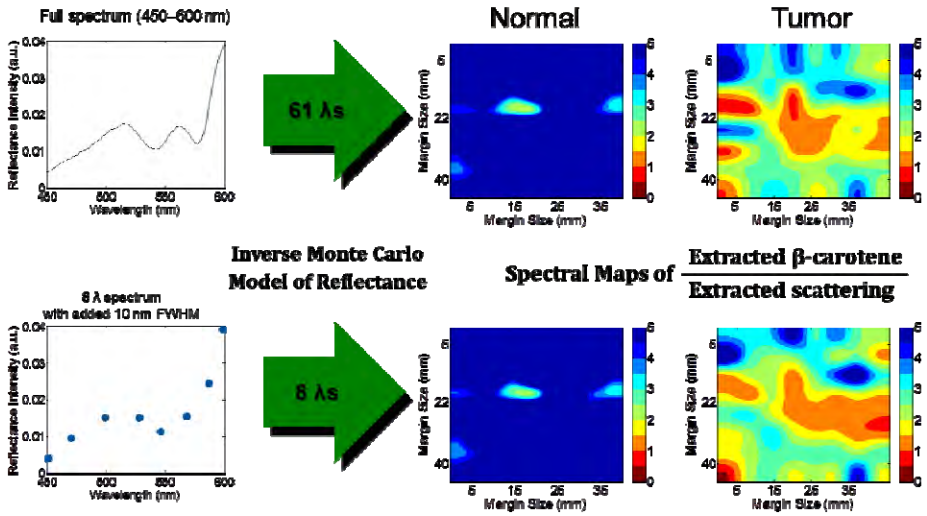

Figure 2.15 – Feasibility of extracting tissue data with a reduced wavelength number

(e) Testing of detector array in biological tissues for SNR

Prior to testing the detector array on human breast tissue samples, we first tested in poultry and bovine samples to ensure that we have adequate SNR. The diffuse reflectance signal photocurrent measured from the animal tissues was normalized with the diffuse reflectance signal measured from a 99% reflectance standard to extract a reflectance contrast image map of the animal tissue. The normalization takes into account the lamp spectrum.

Figure 2.16(a) and (b) show a reflectance contrast image map of the poultry tissue for six discrete wavelengths and a photograph of the imaged sample, respectively. A higher normalized diffuse reflectance photocurrent indicated higher reflectance from the tissue, whereas the lower normalized photocurrent (red) indicated lower reflectance, or higher absorbance. The color contrast present in the tissue photograph correlates well with the reflectance contrast between the pixels. The reflectance contrast map for bovine muscle tissue did not yield any features due to the homogeneous nature of the tissue in that sample.

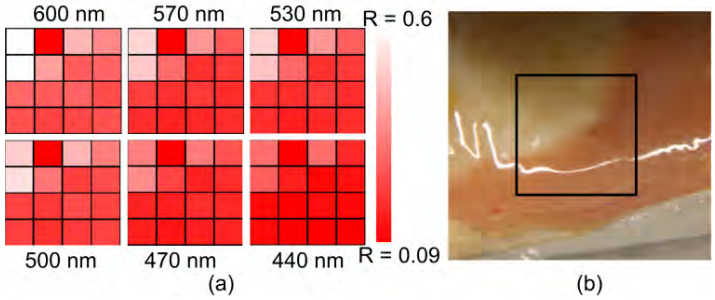

Figure 2.16 – (a) Calculated reflectance contrast image for poultry tissue for discrete wavelengths; (b) photograph of a section of poultry tissue that was imaged by the custom photodiode array

30 repeated diffuse reflectance measurements were taken at each wavelength for every pixel. The SNR was calculated as SNR=20 log (average signal / standard deviation of signals). The SNR estimates for both center and corner pixels were typically between 40 and 60 dB. The bovine tissue exhibited high absorption and thus lower photocurrent and SNR compared to the poultry tissue.

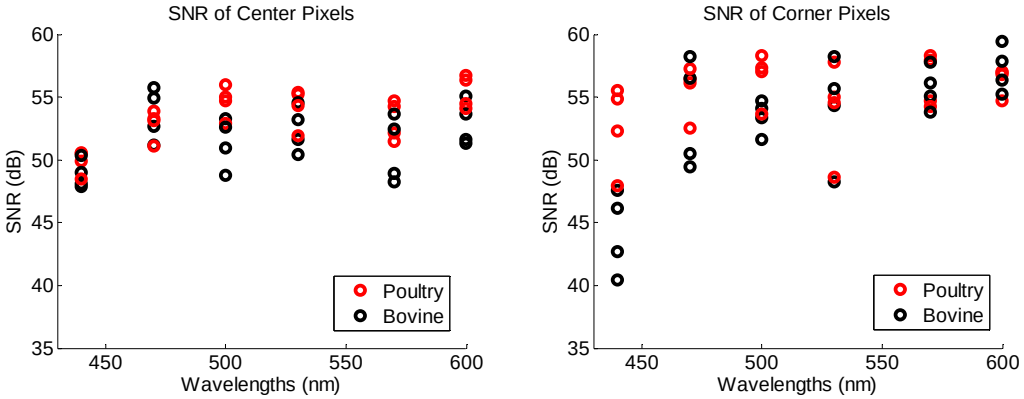

Figure 2.17 – SNR calculations of center and corner pixels on poultry and bovine tissues

From this animal tissue study, we have confidence that this system will have sufficient SNR on human breast tissues. We have finished the sixth year by getting a clinical study in place for using the system on mastectomy and lumpectomy specimens. The system has been tested and approved for clinical and electrical safety. We are currently in the patient recruitment process and will be testing this device at the Duke University Medical Center hospitals in the near future.

3.1 Body Project 2: **Exploiting, physiological, metabolic and molecular contrast in breast cancer**

A. Original SOW for five years

1) *Physiological and metabolic characterization of mammary tumors in an animal model of breast cancer.* Nude mice will be injected in the flank with 500,000 4T1/D2 cancer cells. The tumors will be allowed to grow until they have reached a size of approximately 8 mm in diameter (approximately 1-2 weeks). Non-invasive optical measurements of tumor oxygenation, vascularity and metabolism will be measured using a continuous wave system and compared to independent measurements of tumor hypoxia using an OxyLite fiber optic sensor and immunohistochemistry of hypoxic and metabolic markers (year 1).

2) *Synthesis of contrast agents for molecular imaging.* Gold nanoparticles will be prepared via citrate reduction of chloroauric acid. The particle size will be adjusted to preferentially scatter NIR light. Anti-HER2 and anti-EGFR antibodies will be conjugated to the gold. The scattering spectrum of (1) the pre-labeled nanoparticles will be measured to verify their NIR resonant scattering properties and (2) the labeled nanoparticles to verify binding with the antibodies (a characteristic red-shift in the peak is expected to occur after binding) (year 2).

3) *Molecular imaging in cells*. Human breast cancer cell lines, MDA-MB-468 and SK-BR-3 which over express EGFR and HER2, respectively will be cultured to test the targeting strategies. Cell lines that express low levels of EGFR and HER2 will be used as controls. Each cell type will be labeled according to previously established protocols and imaged using a microscope coupled to a CCD camera. The optical contrast in the cells over expressing HER2 and EGFR receptors relative to that in the control cells will be statistically compared to demonstrate the molecular specificity of the anti-EGFR and anti-HER2 nanoparticles (year 3).

4) *Molecular imaging in animal models.* Tumor cell lines will be stably transfected to over express both HER2 and EGFR, and tumors will be grown in the mammary fat pad of the nude mice used in (a). Both topical and systemic injection of the molecular contrast agents will be explored. An optical imaging system consisting of a tunable laser and a CCD camera will be used to image the molecularly tagged contrast agents for different doses (to measure the effect of dosimetry on the signal to background) as well as for topical vs. systemic delivery. Note that task (a) is directly relevant to this aim as it will provide the instrumentation and algorithms for data analysis as well as experience with the preparation of animal tumor models for these studies (years 4-5).

The original project proposed here has evolved into two distinct projects: (1) The development of techniques to exploit the intrinsic sources of optical contrast (physiologic and morphological) as a means to assess response to cancer therapy and (2) the assessment of extrinsic sources of optical contrast for use as an aid in intra-operative assessment of breast tumor margins.

B. Summary of Accomplishments in years 1 and 2

The goal of this year 1 study was to quantify and track changes in oxygenation in response to carbogen breathing in 4T1 breast tumors in nude mice using optical spectroscopy. Specifically we measured hemoglobin saturation and the optical redox ratio and compared the optical measures of oxygenation to that of a well established method of measuring tumor pO_2, the OxyLite system, to demonstrate the utility of optical spectroscopy to quantitatively monitor tumor physiology in a pre-clinical model. Non-invasive optical spectroscopy was performed on 4T1 breast tumors grown in the flank of nude mice (n=10) before and after the administration of

carbogen (95% O2, 5% CO2), by placing a fiber optic probe in contact with the surface of the tumor.

This work established the ability of optical spectroscopy to consistently track changes in tumor physiology in response to a perturbation. It was found that optical spectroscopy may in fact provide a more robust assessment of tissue oxygenation than the existing Oxylite system, likely due to its larger probing volume. This work establishes optical spectroscopy as a viable tool to monitor changes in tumor physiology in response to other treatments, including radiation, chemotherapy, and molecular therapies, offering many advantages over existing technologies. In particular, it is fast, non-invasive, quantitative, and probes a wide range of physiologic parameters, including blood content, oxygenation, and cellular metabolism. This project has subsequently expanded and will span the full five years of the proposal.

C. Summary of Accomplishments in year 3

Establishing the validity of intrinsic optical biomarkers to quantitatively and longitudinally monitor tumor hypoxia and necrosis in murine tumor models:

Diffuse reflectance spectroscopy was evaluated as a objective tool to assess quantitative physiological changes in solid murine tumor models when exposed to chemotherapy. Specifically, it was investigated whether the optical technique could assess changes in tumor hypoxia and necrosis relative to the traditional immunohistochemical methods. N=50 nude mice were inoculated with 4T1 mouse breast carcinoma cells on their flanks and were evenly distributed into control and treatment groups (each group had 25 animals). The treatment group received an 10 mg/kg of Doxorubicin while the control group received an equivalent volume of saline. The tumors were monitored optically prior to treatment and then for 2 weeks post treatment. Five randomly chosen animals, from each group, were removed for immunohistochemical (IHC) analysis on 4 different days. We found that the optical markers of de-oxygenated hemoglobin and the wavelength-averaged optical tissue scattering coefficient were directly correlated to immunohistochemical assessment of tumor hypoxia and histologically estimated tumor necrosis, respectively. Further we established that the temporal trends in these optical and immunohistochemical parameters were concordant with one another. Another result from this study was that optical measurements indicated a clear and statistically significant increase in the oxygen content in the treated tumors relative to the untreated animals, while both immunohistochemical and tumor growth delay assays showed no differences between the treatment and control groups, lending further credence to the fact that such non-invasive methods may provide both better and earlier indications of treatment effects.

Molecular imaging with 5-ALA:

The research goals for year 3 have changed from the synthesis of scattering contrast agents that was originally proposed to detecting mammary cancer with fluorescent contrast agents. Fluorescence agents were chosen over scattering contrast agents because fluorescence has a unique excitation and emission. In the previous year, aminolevulinic acid (ALA) induced protoporphyrin IX (PpIX) was successfully used to differentiate cancerous cells from normal with fluorescence lifetime. This work was carried on into the beginning of this year by examining fluorescence intensity and spectroscopy. It was found that PpIX has a significantly greater fluorescence increase in malignant cells as compared to normal cells. However, the raw fluorescence intensity of cells cannot be used to delineate malignant from normal without a fluorescence control to determine the endogenous fluorescence. The long incubation time, 2 hours, and endogenous fluorescence required to detect PpIX is clinically prohibitive. It was concluded that for clinical use within the operating room, PpIX is not ideal.

D. Summary of accomplishments in year 4-5

Using optical spectroscopy to assess early response to radiotherapy using intrinsic optical biomarkers

In this year, we evaluated if diffuse reflectance spectroscopy could be used as an objective tool to assess early response in solid murine tumors model that were exposed to radiotherapy. The non-invasive and quantitative nature of this technique along with its ability to performed using a variety of different fiber-optic probe geometries makes it highly relevant to translational applications. We have completed a preliminary animal study to explore the feasibility of using optical biomarkers obtained early during a course of curative radiotherapy in predicting long term local tumor control. N=34 nude mice were inoculated with 10^6 FaDu human hypopharyngeal squamous cell carcinoma cells, subcutaneously, on their right flanks. Once the average tumor diameters reached 6-8 mm, the animals were evenly distributed by tumor volume into control and treatment groups in a 1:2 ratio, respectively. N=23 animals in the treatment group were exposed to 39 Gy of radiation, while N=11 animals in the control group received sham irradiation. The dose of 39 Gy was chosen as it has previously been reported as the TCD_{50} (dose which provides local control to 50% of the treated population) for this tumor model in nude mice. Treatment day was labeled day 0. All tumors were monitored optically before treatment to get baseline measurements on day 0 and then again on days 1, 3, 5, 7, 10, 12, 14 and 17. Tumor volumes were measured once using calipers each day over the course of the optical measurements and then one or two times per week until 120 days post treatment.

This study was one of the first of its kind to demonstrate the predictive ability of a non-invasive sensing method to select animals that had complete local control relative to animals that fail treatment. We observed that animals showing complete local control (as defined by the lack of a palpable/visible lesion 120 days post treatment) showed statistically significant rates of increase in tumor oxygen saturation as early as 7 days post-irradiation, relative to the subjects that failed treatment. These responding animals also maintained higher levels of tumor oxygen saturation relative to the animals that failed treatment up to 17 days post-treatment. We have been able to build preliminary linear discriminant models that were able to separate the animals that responded to the treatment vs. not with 100% sensitivity and 85% specificity.

Molecular imaging of tumor metabolism

One physiological endpoint that we have been interested in measuring is tumor metabolism. A number of studies have discussed and hypothesized the role cellular metabolism plays in determining a cell's propensity for aggression. To identify a possible link between metabolism and cell behavior, we measured the optical redox ratio from a panel of human breast cancer cells. The optical redox ratio is defined as the ratio between two endogenous fluorophores – NADH and FAD that play a critical role in cellular metabolism. Given that tumor aggression in breast cancers was linked to estrogen receptor status, we stratified the cell lines selected based on estrogen receptor (ER) status. We observed a statistically significant increase in redox ratio of ER(+) breast cancer cells. Interestingly, the redox ratio was also significantly higher for ER(+) cells compared to ER(-) cells. Treatment with Tamoxifen, a known glycolytic inhibitor, significantly reduced the redox ratio of Er(+) cells. These results show significant promise that cellular metabolism could be used to ascertain the behavior of breast cancers and help predict their long-term behavior.

In addition to measuring endogenous fluorescence markers indicative of cell metabolism, we also explored the utility of exogenous agents that could indicate glucose demand oruptake in cells and tumors. Specifically, we explored the feasibility of using 2-[*N*-(7-nitrobenz-2-oxa-1,3-diazol-4-yl)amino]-2-deoxy-D-glucose, (2-NBDG) to measure glucose uptake in cells. We found that much like glucose, 2-NBDG also required GLUT 1 for entering a cell. Here, GLUT 1 refers to the membrane protein that mediates glucose uptake in a cell. We found significantly higher 2-NBDG uptake in breast cancer cells as compared to human mammary epithelial cells (HMEC). In addition, when administered with glycolytic activators or inhibitors, 2-NBDG fluorescence increased or decreased, respectively. Specifically, 2-NBDG uptake was measured in response to anti-cancer therapies lonidamine (LND) and alpha-hydroxycinnamate (a-Cinn). LND directly inhibits hexokinase II, the enzyme that converts glucose in a cell to glucose-6-phosphate and initiates glycolysis. Similarly, a-cinn increases the need for glucose and was found to cause an increase in 2-NBDG. When treated with Tamoxifen, a commonly used endocrine therapy for breast cancer, estrogen receptor positive breast cancer cells took up significantly lower 2-NBDG compared to ER- cells. Our results agree with the expected response to tamoxifen, which is a known glycolytic inhibitor in breast cancer cells. Our results demonstrate the potential of 2-NBDG for 1) testing the efficacy of drugs that target glycolysis and 2) tracking metabolic demand in cells.

E. Progress report for year 6

One of the most intriguing characteristics of a cancer cell is its ability to survive in a harsh microenvironment that is otherwise toxic to normal cells. In spite of the lack of oxygen and severely acidic extracellular space that is typically representative of tumor microenvironment, cancer cells manage to generate enough energy to survive, proliferate and eventually metastasize. A number of *in vitro* and *in vivo* studies have identified a link between hypoxia and metastasis and resistance to radiotherapy.

Interestingly, two distinct types of hypoxia are observed *in vivo*: cycling hypoxia and chronic hypoxia. Cycling hypoxia—periods of hypoxia broken up by periods of reoxygenation— occurs because of temporal instabilities in red blood cell flux, often as a result of angiogenesis. Chronic hypoxia is an extended lack of oxygen, usually resulting from tumor cells outgrowing the oxygen limit of their blood supply. Although both types of hypoxia characterize tumors, each leads to distinct outcomes. Cycling hypoxia is associated with poor prognosis and has been shown to lead to metastasis, radioresistance, and chemoresistance, among other factors. The prognosis is much better for chronic hypoxia, as it has been correlated with increased efficacy of radiation therapy. However, the specific reasons why one form of hypoxia is likely to confer radioprotection and cause metastasis remain unexplored. Given that oxygen, or lack thereof, is a key player in determining the energy pathways of a cell, the metabolic response to hypoxia could provide significant insight into long-term tumor behavior.

In Year 6, we have started to use 2-NBDG as a marker of glycolytic demand in cells that are exposed to different forms of hypoxia. Specifically, we compared the effect of chronic as well as cycling hypoxia on 2-NBDG uptake in cells. These experiments represent a long-term effort to study the effect of duration, frequency and reoxygenation period on glycolytic demand in cancer cells. Using 2-NBDG and endogenous metabolic markers, we aim to determine if a cell's short-term response to hypoxic stress is indicative of its long-term outcome. By nondestructively correlating a cell's environmental stress (hypoxia) with metabolic endpoints (NBDG and NADH fluorescence), we hope to gain valuable information that may assist in predicting a tumor's

future behavior. Determining hypoxic response and metabolic status may provide the first step in predicting a cancer's aggressiveness and it's response to therapy.

Study Design

Comparison of Normoxia, Chronic Hypoxia, and Cycling Hypoxia

The cell line used was 4T1-RFP, a murine mammary cancer cell line transfected with constitutively expressed red fluorescent protein. Using 4T1-RFP cells allows us to confirm the presence of cells by viewing the red fluorescence during imaging, and the same cell line can be easily transitioned to a small animal model.

The cells were subjected to one of three hypoxic perturbations: normoxia (20% O2), chronic hypoxia (3 hours at 0.5% O2), or cycling hypoxia (1 hour at 0.5% O2 followed by 1 hour at 20% O2 for three cycles). After the perturbation, cells were removed from hypoxia and kept at 20% O2. Cells were then imaged at selected timepoints (0, 1, 2, 3, 4, 6, 8, 12, 18 and 24 hours), as shown in Figure 3.1

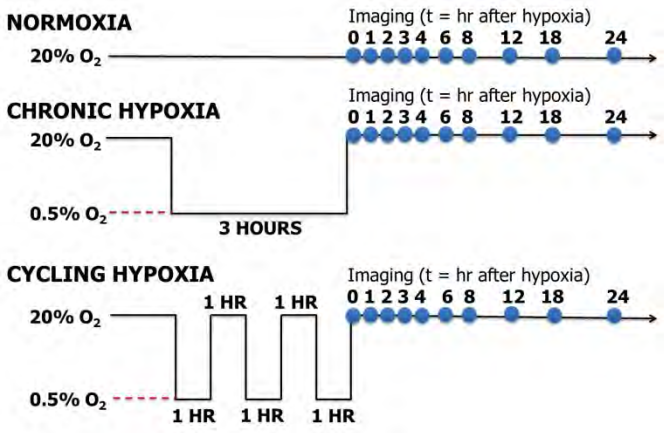

Figure 3.1. 4T1-RFP cells were subjected to one of three hypoxic perturbations. Cell plates were then imaged at specified timepoints up to 24 hours post-hypoxia.

Before imaging, each cell plate was washed 2x with PBS and incubated for 20 minutes with 3mL of 100uM 2-NBDG. The cells were washed twice more with PBS and then imaged in PBS. Two-photon imaging was used to achieve depth-resolved images. Excitation was at 920nm and emission was collected from 495-540nm (2-NBDG) and 575-630nm (RFP). Background-subtracted images were analyzed using Matlab software to obtain average per-pixel fluorescence intensity value Images were normalized using the average background intensities to account for day-to-day system variations.

Comparison of Normoxia, Chronic Hypoxia, and Cycling Hypoxia

After the perturbation, 2-NBDG uptake was quantified and compared across groups at each timepoint. A representative two-photon image for each experimental group is shown in Figure 3.2.

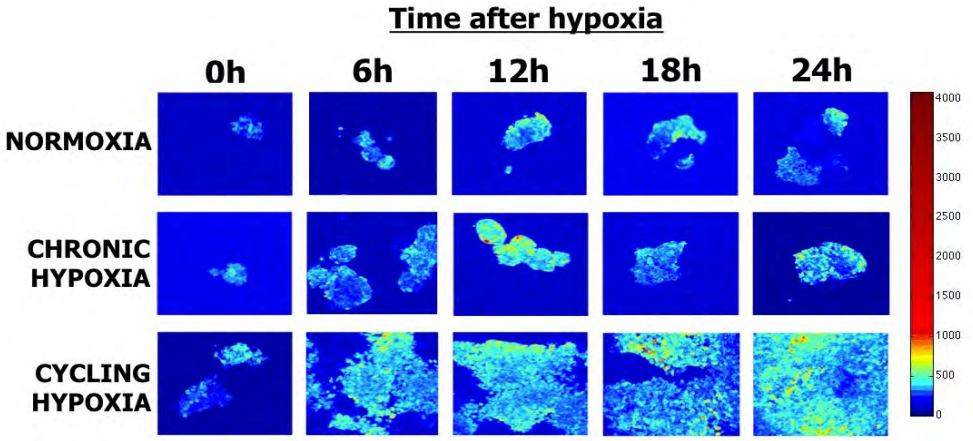

Figure 3.2: Representative two-photon images show 2-NBDG fluorescence in cells. Cells were excited at 920nm and two-photon emission was collected from 495-540nm.

The quantified fluorescence intensity for each group is shown in Figure 3.2. As evidenced by the graph, NBDG fluorescence increased significantly ($p<0.02$) after cycling hypoxia at all timepoints except t=18h. The chronic hypoxia group was statistically indistinguishable from the normoxic control at all timepoints except for t=24h ($p<0.01$). At t=24h, the chronic hypoxia-treated group displayed a fluorescence intensity similar to the cycling hypoxia group. The reason for this jump has not yet been determined, but will be explored further in future experiments. The large standard deviations in some of the experimental groups may be due to the small imaging field of view. However, we note that the observed trends were representative of the entire imaging area. These preliminary results indicate that 2-NBDG may be able to track metabolic changes that result from hypoxic stress.

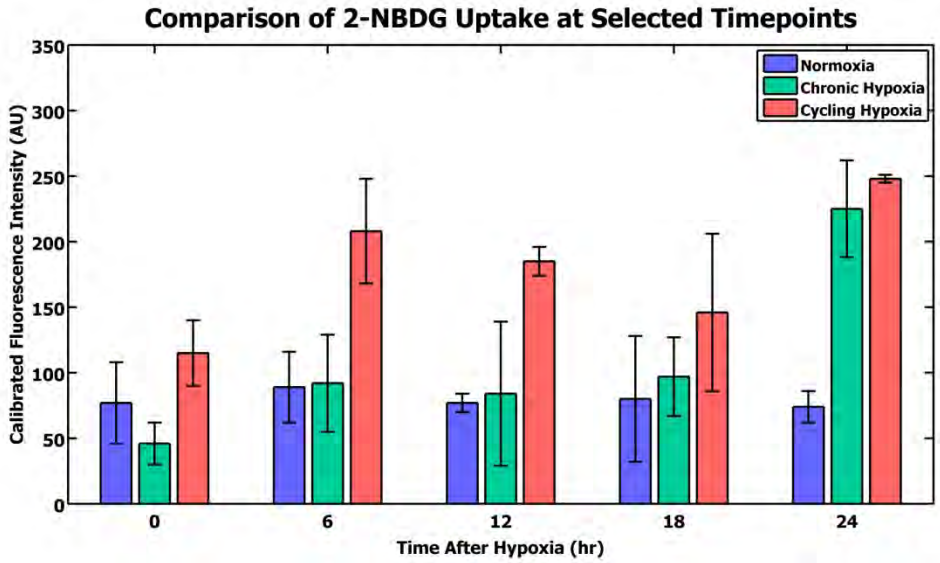

Figure 3.3**:** Changes in 2-NBDG uptake were seen in response to hypoxic stress. Cycling hypoxia caused significant increase in uptake at all timepoints except t=18h ($p<0.02$). Chronic hypoxia was distinguishable from the normoxic control at t=24h ($p<0.01$). Error bars represent standard deviation.

Plans for Continued Work

We plan to continue using NBDG to study the effects of hypoxia on metabolism in 4T1-RFP cells. We are currently performing a hypoxic dose experiment to correlate the duration of hypoxia with metabolic changes. Future results from this experiment will include optically measuring NADH (as described in Ostrander et al. Cancer Research 2010), performing Western blots to measure nuclear expression of hypoxia and glycolysis related transcription factors.and quantifying 2-NBDG uptake at each timepoint. This study will be repeated for both cycling and chronic hypoxia. We will then expand the study to include reoxygenation after hypoxia.

Further, we will explore different models for testing our hypotheses. The experiment will be expanded to study a panel of human breast cancer cell lines of varying endocrine status. Establishing a "library" of stress response and metabolic behavior may provide useful information for predicting a cancer's aggressiveness and planning appropriate therapy.

3. KEY RESEARCH ACCOMPLISHMENTS

Project 1. System-on-a-chip device

- Design, fabrication, and testing of several single-pixel photodiode-based prototypes
- Determined that an annular photodiode with central illumination geometry will maximize throughput and SNR
- Showed that diffuse reflectance spectroscopy alone can achieve high sensitivity and specificity for discriminating malignant from nonmalignant breast tissues
- Developed a 3x3 fiber-illumination/photodiode-based spectral imaging probe and extracted optical properties from liquid phantoms with high accuracy (errors < 10%)
- Developed a free-space back-illumination strategy to further reduce the footprint of the system by eliminating optical fiber bundles
- Fabricated annular silicon photodiode arrays in-house that has comparable performance to commercially available photodiodes to better model the probe geometry
- Designed a slab-waveguide for uniform illumination of the sample and simulated the theoretical throughput of the light delivery system
- Designed and built a new integrating transimpedance amplifier circuit to reduce noise and increase SNR of the overall system
- Showed feasibility of extracting physiological parameters with comparable values as the benchtop system while reducing number of wavelengths and increasing bandpasses at each center wavelength
- Showed feasibility of using photodiode-based system by testing on bovine and poultry tissue for SNR

Project 2. Exploiting, physiological, metabolic and molecular contrast in breast cancer

- 2-NBDG was used to observe metabolic changes in response to hypoxia.
- After cycling hypoxia, 2-NBDG uptake was shown to increase significantly.
- Preliminary results show that 2-NBDG uptake may be different in response to chronic hypoxia versus cycling hypoxia.

4. REPORTABLE OUTCOMES

Project 1. System-on-a-chip device

1) Dhar S, Lo JY, Yu B, Brooke MA, Ramanujam N, Jokerst NM, “Custom annular photodetector arrays for breast cancer margin assessment using diffuse reflectance spectroscopy,” *Proceedings of IEEE Biomedical Circuits and Systems*, accepted 2011.

2) Dhar S, Lo JY, Yu B, Tyler T, Brooke MA, Kuech TF, Ramanujam N, Jokerst NM, “A custom wide-field spectral imager for breast cancer margin assessment,” *Proceedings of IEEE Photonics Society Annual Meeting*, accepted 2011.

3) Lo JY, Yu B, Kuech TF, Ramanujam N. “A compact, cost-effective diffuse reflectance spectroscopic imaging system for quantitative tissue absorption and scattering,” *Proc. of SPIE* Vol 7890, 2011.

4) Lo JY, Dhar S, Yu B, Brooke MA, Kuech TF, Jokerst NM, Ramanujam N. “Design, validation, and implementation of a diffuse reflectance spectroscopic imaging system for tissue absorption and scattering,” *Proceedings of SPIE Photonics West*, accepted 2011.

5) Fu HL, Yu B, Lo JY, Palmer GM, Kuech TF, Ramanujam N, "A Cost-Effective, Portable, and Quantitative Spectral Imaging System for Application to Biological Tissues" *Optics Express*, Vol. 18, Issue 12, pp. 12630-12645, 2010.

6) Lo JY, Yu B, Fu HL, Bender JE, Palmer GM, Kuech TF, Ramanujam N. "A strategy for quantitative spectral imaging of tissue absorption and scattering using light emitting diodes and photodiodes." *Optics Express*. 17 (3):1372-1384, 2009.

7) H.L. Fu, B. Yu, J.Y. Lo, T.F. Kuech, and N. Ramanujam, “A Low Cost System for Quantitative Spectral Imaging of Tissue Absorption and Scattering,” ECI Conference on Advances in Optics for Biotechnology, Medicine and Surgery XI *Clinical Challenges and Research Solutions,* June 28 - July 2, 2009, Burlington, Vermont, USA.

8) Yu B, Lo JY, Palmer GM, Bender JE, Kuech TF, Ramanujam N. “A cost-effective diffuse reflectance spectroscopy device for quantifying tissue absorption and scattering *in vivo*,” *Journal of Biomedical Optics*. 13 (6): 060505, 2008.

9) Lo JY, Yu B, Palmer GM, Kuech TF, Ramanujam N. “A Miniature Optical Device for Noninvasive, Fast Characterization of Tumor Pathology,” Biomedical Optics, *OSA Technical Digest*, BTuF55, 2008.

Project 2. Exploiting, physiological, metabolic and molecular contrast in breast cancer

1) Rajaram N, Fontanella AN, Frees AE, Jiang TT, Millon SR, Hansen K, Brown JQ, Dewhirst MW, Ramanujam N. Optical imaging of tumor metabolic response to hypoxia. *(in preparation)*, 2011

2) Rajaram N, Frees AE, Millon SR, Fontanella AN, Dewhirst MW and Ramanujam N. Effect of intermittent hypoxia on vascular oxygenation and tumor glycolytic demand in pre-clinical breast cancer models. Department of Defense Era of Hope Conference, Orlando, FL, Aug 2-5, 2011.

3) Rajaram N, Frees AE, Jiang TT, Millon SR, Fontanella AN, Dewhirst MW and Ramanujam N. Optical imaging of tumor metabolic response to hypoxia. ECI Advances in Optics for Biotechnology, Medicine and Surgery, Naples, FL, June 5-8, 2011. **Best Talk Award**

4) Frees AE, Rajaram N, Jiang T, Millon S, Dewhirst M, Ramanujam N. "Utilizing 2-NBDG Fluorescence to Study Hypoxia-Induced Changes in Breast Cancer Glycolysis." ECI Advances in Optics for Biotechnology, Medicine and Surgery, Naples, FL, June 5-8, 2011. **Best Poster Award**.

5) Vishwanath K, Palmer GM, Brown JQ, Ramanujam N, "Non-invasive and quantitative sensing of tumor physiology and function via steady-state diffuse optical spectroscopy " in Biosensors and biodetection technologies for cancer detection, diagnostics and research, Rasooly, A. and Herold, K., ed. (CRC Press, in press).

6) Vishwanath K., Salama J, Walter L, Dewhirst MW, and Ramanujam N. "Non-invasive longitudinal assessment of tumor oxygenation in-vivo in irradiated head and neck human cancers using diffuse reflectance spectroscopy," in ECI conference Advances in Optics for Biotechnology, Medicine and Surgery XII, 2011.

7) Millon SR, Ostrander JH, Brown JQ, Rajeha AM, Seewaldt VL, Ramanujam N. "Uptake of 2-NBDG as a method to monitor therapy response in breast cancer cell lines." Breast Cancer Research and Treatment 126(1): 55-62, 2011.

8) Ostrander J H**,** McMahon CM, Lem S, Millon SR, Seewaldt VL, Ramanujam N. The Optical Redox Ratio Differentiates Breast Cancer Cell Lines Based on Receptor Status. Cancer Research. 70(11), 4759-4766. 2010.

9) Millon SR, Ostrander JH, Yazdanfar S, Brown JQ, Raheja AM, Ramanujam N. "Preferential accumulation of 5-aminolevulinic acid-induced protoporphyrin IX in breast cancer: A comprehensive study on six breast cell lines with varying phenotypes." Journal of Biomedical Optics. 15(1): 018002. 2010.

10) Millon SR, Ostrander JH, Brown JQ, Ramanujam N. "Uptake of 2-NBDG in normal mammary epithelial and breast cancer cells." ECI Advances in Optics for Biotechnology, Medicine and Surgery, Naples, FL, June 28 - July 2, 2009.

11) Millon SR, Ostrander JH, Brown JQ, Ramanujam N. "2-NBDG for use in breast cancer detection and therapy monitoring in vitro." Fitzpatrick Symposium: Frontiers in Photonics and Science 2009.

12) Millon SR, Ostrander JH, Brown JQ, Ramanujam N. "2-NBDG for use in breast cancer detection and therapy monitoring in vitro." Duke Comprehensive Cancer Center Annual Meeting. (2009).

13) Vishwanath K, Huan Y, Barry WT, Dewhirst MW, and Ramanujam N. Using Optical Spectroscopy to Longitudinally Monitor Physiological Changes within Solid Tumors. *Neoplasia* **11**, 889-900. 2009

14) Vishwanath K, Klein D, Chang K, Schroder T, Dewhirst M, and Ramanujam N. Quantitative optical spectroscopy can identify long-term local control in irradiated murine head and neck xenografts. *J Biomed Opt* 14(5), 054051. 2009

15) Million SRC, Ostrander JH, Brown JQ, Ramanaujam N. “Fluorescence analysis of the effect of 5-aminolevulinic acid on the PpIX induced fluorescence of normal and malignant breast cell lines.” NIBIB Training Grantees Meeting. Bethesda, MD. June 2008.

16) K. Vishwanath, H. Yuan, L. Moore, J. Bender, M. Dewhirst, N. Ramanujam. "Longitudinal Monitoring of 4T1-Tumor Physiology *in vivo* with Doxorubicin Treatment via Diffuse Optical Spectroscopy," Optical Society of America: Biomedical Optics Topical Meeting, St. Petersburg, FL, Mar., 2008.

17) Millon SR, Provenzano PP, Elicieri KW, Brown JQ, Keely PJ, Ramanujam N. "Imaging of ALA-induced PpIX in normal and malignant breast cells". Engineering Conferences International: Advances in Optics for Biotechnology, Medicine and Surgery. Naples, FL, June 2007.

5. CONCLUSIONS

A. Project 1. System-on-a-chip device

In our original statement of work, we proposed to measure the fluorescence of *ex vivo* human breast tissues with a system-on-a-chip device. Throughout the duration of the grant, we found through other clinical studies that we are able to achieve comparable sensitivity and specificity with diffuse reflectance alone. We turned our focus to system miniaturization by re-designing the detection and illumination strategies of the device.

We used commercially available photodiodes to test the fundamental concept of whether or not we can extract optical properties with high accuracy when we remove the sophisticated and expensive CCD and spectrograph. We eliminated the optical fiber bundles from our system by using a free-space approach, and we struggled to get sufficient throughput and SNR. To mitigate this problem, we designed a new integrating transimpedance amplifier circuit to better detect low photocurrents from the photodiode and thus improved the SNR. We have also continued to develop new light delivery systems in parallel to accomplish the same goal. In the latter years of the grant, we have developed new photodiode fabrication processes to customize the detector geometry to better model the device. With the ability to fabricate the detectors into any geometry, there is added potential for many other applications that require different sensing depths into tissues.

We were unable to test the miniaturized system on clinical samples by the end of this grant. However, we were able to essentially reduce the footprint of a conventional fiber-based spectral imaging system by 99.3% and the cost by ~90%. We will continue to develop and optimize this miniature spectral imaging system and apply it in a clinical setting through other means of funding in the near future.

A. Project 2

a. Molecular imaging with NBDG

Preliminary results indicate that 2-NBDG may be a valuable tool for assessing a cell’s response to hypoxic stress. Cells were subjected to normoxia (control), chronic hypoxia, or cycling hypoxia and then treated with 2-NBDG at various points during reoxygenation. Cycling hypoxia significantly increased 2-NBDG fluorescence intensity at nearly all timepoints ($p<0.02$). Though chronic hypoxia initially caused little change in 2-NBDG uptake, 2-NBDG fluorescence intensity spiked at t=24h ($p<0.01$). We will continue to use 2-NBDG to determine a cell’s metabolic response to hypoxia and reoxygenation. Non-destructive determination of metabolic state using NBDG has the potential to be a valuable tool for predicting a tumor’s long-term behavior.

6. INDIVIDUALS RECEIVING PAY FROM RESEARCH EFFORT

Nimmi Ramanujam
Gregory Palmer
Bing Yu
Karthik Vishwanath
Narasimhan Rajaram
Justin Lo
Henry Fu
Janelle Bender
Stacy Millon
Lee Wilke
Mark Dewhirst
Thomas Kuech
Elizabeth Burnside
Josephine Harter
Ning Liu

7. REFERENCES

1. Yu, B. and N. Ramanujam, *A Cost-Effective Diffuse Reflectance Spectroscopy Device for Quantifying Tissue Absorption and Scattering In Vivo.* Opt Lett, 2008.
2. Zhu, C., Palmer GM, Breslin TM, Harter JM, Ramanujam N, *Diagnosis of Breast Cancer using Fluorescence and Diffuse Reflectance Spectroscopy: a Monte Carle Based Approach.* J Biomed Opt, 2008. **13**(3): p. 034015.